Available online at www.sciencedirect.com

jmr&t Journal of Materials Research and Technology

journal homepage: www.elsevier.com/locate/jmrt

Original Article

Alternative fractional crystallization-based methods to produce high-purity aluminum

Danilo C. Curtolo [1], *Martin J. Rodriguez-Rojas* [1], *Semiramis Friedrich* [*,1], *Bernd Friedrich*

IME Institute of Process Metallurgy and Metal Recycling, RWTH Aachen University, Germany

ARTICLE INFO

Article history:
Received 8 October 2020
Accepted 5 March 2021
Available online 13 March 2021

Keywords:
High purity aluminum
Fractional crystallization
Zone melting
Cooled finger

ABSTRACT

The increasing demand of ultra-high purity aluminum for technological applications has triggered the improvement of purification methods during the recent decades. Some of the most relevant applications for ultra-high purity aluminum include electrolytic condensers, transistors, integrated circuit conductors, magnetic disks substrates and low-temperature superconducting magnets. The most commonly used industrial technique for refining high purity aluminum is the three-layer electrolytic process, reaching purification levels of up to 4N8 (99,998 wt.%). An alternative and less capital intensive method to achieve such purification level is fractional crystallization. While the three-layer electrolytic process remains almost unchanged among its proprietaries, the fractional solidification processes vary considerably on their techniques and setups used to achieve an efficient segregation of impurities from the base metal. The purpose of this article is to compare the cooled finger and zone melting, two existing fractional crystallization methods, available at the Institut für Metallurgische Prozesstechnik und Metallrecycling (IME) of the RWTH Aachen University. The purification effect caused by different types of convection from these two fractional crystallization techniques was experimentally shown and the common characteristics among fractional crystallization equipment; i.e. growth rate, thermal gradient and purification rate, were investigated. The competitive advantage of the cooled finger over zone melting was demonstrated. Although both techniques are capable of refining aluminum, the design of the cooled finger favors a better impurity segregation.

1. Introduction

The usage of ultra-high purity aluminum (over 99.998 wt.% Al, aka 4N8-Al) is mostly concentrated in the electronic- and semiconductor industry. One of its most important applications is in integrated circuits (IC) fabrication. Within the IC fabrication environment, high purity aluminum oxide (Al_2O_3) is used as a tough, electrically insulating and inert coating on the surfaces of the semiconductor's production equipment

* Corresponding author.
E-mail address: SFriedrich@ime-aachen.de (S. Friedrich).
[1] These authors contributed equally to this work.

https://doi.org/10.1016/j.jmrt.2021.03.025

[1,2]. Also in this field, 5 N purity aluminum with extremely low contents of Thorium (Th) and Uranium (U) is used in the production of transistor interconnects, including the fabrication of bonding wires for semiconductor packaging. These applications rely on aluminum's inherent high electrical conductivity and thin electrical insulation layer of oxide formed on its surface. The low amount of Th and U is necessary to prevent signal disturbances [3].

In electronic industry –the biggest consumer –an anode foil made of ultra-high purity aluminum is used in the fabrication of electrolytic capacitors due to the high volumetric efficiency (high capacitance per volume). Additional applications that require purification levels up to 6 N include magnetic disk substrates, sputtering targets, liquid crystal display (LCD) panels, cathodes for organic light emitting diode (OLED) displays, high purity alumina production and as electrical and thermal conductor for low temperatures superconducting magnets [1,4–6].

1.1. *Current industrial production*

Most industrially used techniques for the production of high purity aluminum includes the three-layer electrolytic process –also known as Hoopes process –and the segregation process. Starting from primary aluminum (3 N), both process can achieve purity levels up to 4N8. To reach the purity levels of 6 N and higher, the segregation process is commonly preferred over vacuum distillation or other complex routes [3,7–12].

The three-layer electrolysis method is based on the transport of aluminum through an electrolyte placed between an alloy containing primary aluminum (3 N) and the high purity (4N8) aluminum output layer. In this process, an Al- ~35wt.% Cu alloy with the density of around 3.0 g cm^{-3} remains at the bottom of the electrolysis cell serving both as anode and the source of aluminum. A molten salt electrolyte with the density of 2.7 g cm^{-3} allows the aluminum ions to flow through, while serving as a physical barrier to avoid the contamination of the purified aluminum ($\rho = 2.3$ g cm^{-3}) with the anode layer. Since the aluminum in the bottom alloy is continuously transported through the electrolyte, more aluminum needs to be charged at the same rate as it is being deposited [13].

The three-layer electrolytic process has been a successful method to produce high volumes of high purity aluminum up to 4N8 levels. However, the constant increase in energy costs as well as the growing pressure to reduce CO_2 emissions has driven the industry to migrate to a more suitable method for the high purity aluminum production. Meeting these needs, the segregation process is a viable candidate that has been widely used as an alternative process or as the part of the high purity aluminum process chain (See Fig. 1) [2,13].

The segregation is a purification method, in which the molten aluminum is kept slightly above its melting temperature and then slowly solidified, to crystallize a new solid with lower impurity levels than its initial concentration. The mechanism behind the segregation process is the fractional crystallization and is characterized by the difference in the solid solubility of impurity elements in aluminum. When slowly crystallized, the eutectic impurities present in the primary aluminum (mainly Si, Fe, Cu, Mg, Ni, Zn, Ga, and

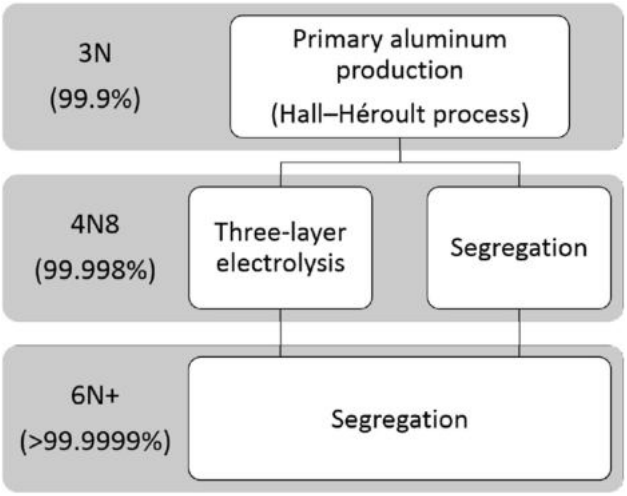

Fig. 1 – High purity aluminum production process flow.

specially for electronic applications U and Th) will tend to remain in the molten phase rather than in the solid phase. When a portion of molten aluminum is crystallized, this will have a higher purity than the initial aluminum while the remaining liquid will contain most of the impurities [1].

1.2. *Fractional crystallization mechanism*

The fractional crystallization is a natural phenomena that occurs when a metal is slowly solidified in a controlled manner. Upon solidification, the solutes that have their distribution coefficients k lower than the unit (Eq. (1)), will tend to remain in the molten phase, while the ones with values higher than one will be incorporated into the forming crystal. This physical phenomenon, by which solutes are rejected from the forming crystals into the melt, is what provides fractional crystallization its purifying characteristic. This process can be progressively performed over previously purified solids, to further increase their purity level by removing the solute enriched portion. The incorporation of impurities from the liquid into a solid can be described in Eq. (1) by the distribution coefficient [14].

$$k = C_S/C_L \quad (1)$$

where, k is a dimensionless factor, C_S is the solute concentration in the solid, and C_L is the solute concentration in the liquid. The distribution coefficient of the two most common impurities present in aluminum is shown in Table 1 [15].

When solidification occurs very slowly, the composition of the forming crystals follows the solid concentration CS = k • CL, assuming that the diffusion in the solid is negligible. Since the rejected solutes become enriched in the melt as

Table 1 – Distribution coefficient of the main impurities in aluminum.

Element	Fe	Si
Distribution coefficient (k)	0.018–0.053	0.082–0.12

crystallization continues, the solids formed in later stages will also become richer in solutes [19]. Assuming no diffusion in the solid and a total mixing in the liquid, the solute enrichment throughout the solidification process can be well described by the Scheil's equation as shown in Eq. 2 [14].

$$C_S = k \cdot C_0 \cdot (1 - f_s)^{k-1} \quad (2)$$

where, f_s is the solidified fraction of the melt and C_0 is the initial solute concentration.

If on the other hand, no mixing is considered in the liquid and only diffusion act as the solute transporter at solidification interface, as solidification proceeds, the rejected solutes will no longer be able to diffuse fast enough to form a homogeneous solute concentration in the melt. Instead, they will form a solute layer with a concentration gradient ahead of the solidifying front.

To account for the variation in solute concentration ahead of the solidifying front, one may consider an effective distribution coefficient (K_{eff}) which will depend on the solute transport process within the melt and the solute rejection occurring at the solidifying front. The effective distribution coefficient –as firstly proposed by Burton, Prim and Slichter–considers a thin diffusion layer ahead of solidification front. Within this layer, the solute transport out of the solidification front is driven by diffusion. This diffusion layer can be influenced by the kinetic aspects of the process. As described in Eq. (3), in order to improve the solute rejection of a given impurity, one can decrease the solid growth rate (V) and reduce the thickness of the diffusion layer (δ) [14,16–18].

$$k_{eff} = \frac{k}{k + (1 - k) \cdot e^{[-V\delta/D]}} \quad (3)$$

where, k is the distribution coefficient, V the solid growth rate, δ is the thickness of the diffusion layer and D is the solute diffusion coefficient in the liquid.

While reducing the solid growth rate is a viable alternative to allow the necessary time for the solute to surpass the diffusion layer and migrate to the molten phase, the decrease of this layer thickness has proved to be an effective method to improve the rejection of solute to the melt while keeping the growth rate -and therefore productivity-at relatively high levels.

The reduction in the diffusion layer thickness can be performed by promoting a forced mix of the molten phase near the solidification growth front and can be achieved by e.g. forced convection, cavitation via ultra-sound, and electromagnetic fields [14,19–22].

1.3. *Cooled finger as an efficient alternative to zone melting*

Since it's development in the 1950s, zone melting has been the most used technique for the fractional crystallization of aluminum. The success behind the wide adoption of this technique relies on the its simplicity. Basically, it functions by creating a molten zone which moves along a metallic bar. This molten zone is created by an external heat source, that can be either a resistance heater or an inducing coil (see example of Fig. 2 for a inductively heated zone melting equipment).

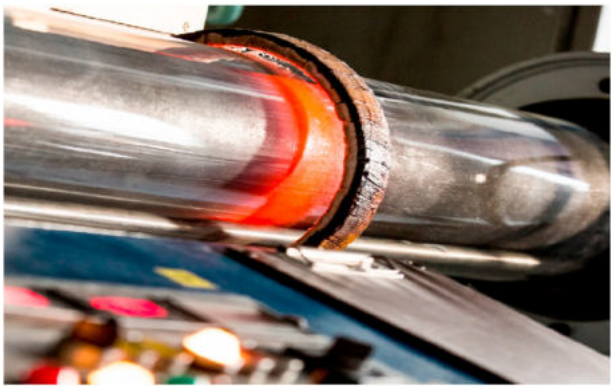

Fig. 2 – Induction heated zone melting located at IME institute, RWTH Aachen University (Photo by Martin Braun).

The temperature gradient profile within the molten zone is responsible for the convection, which assists the decrease in the diffusion layer thickness, according with the solute segregation theory proposed by BPS. When an induction heating system is employed, the added electromagnetic stirring adds up to the overall mixing at the solidification front.

Despite the wide usage of zone melting as the standard technique for the purification of aluminum, the development of the cooled finger as a fractional crystallization method, based on a Japanese patent from 1980's, provides a competitive advantage over the zone melting equipment [23].

The cooled finger purification equipment, consists of a double-wall fluid-cooled rotating shaft that solidifies a crystal inside the melt. The mechanical mixing provided by the rotation of the cooled finger, creates a strong fluid velocity with its peak intensity directly ahead of the solidification front.

In zone melting the mixing caused by the sum of both thermal and electromagnetic convection generates its highest intensity between the center of the molten zone and the solidification front. In Fig. 3 the different forms of convection are shown for both techniques, resulting in a different flow velocity profile.

The fluid flow behavior is one of the most important aspect in fractional crystallization, as it is related to the temperature distribution in the system as well as to the mass transport within the melt. Generally, the fluid flow enhances the mass transfer by transporting away the melt from the solid–liquid region (containing high concentration of segregated impurities), and replacing it with "fresh" material containing lower amount of impurities [24].

The assumption is that the mechanical stirring created by the cooled finger has a greater effect on decreasing the diffusion layer thickness (shown as a blue interface in Fig. 3), which improves the impurity segregation, while increasing the purification efficiency of this technique [24].

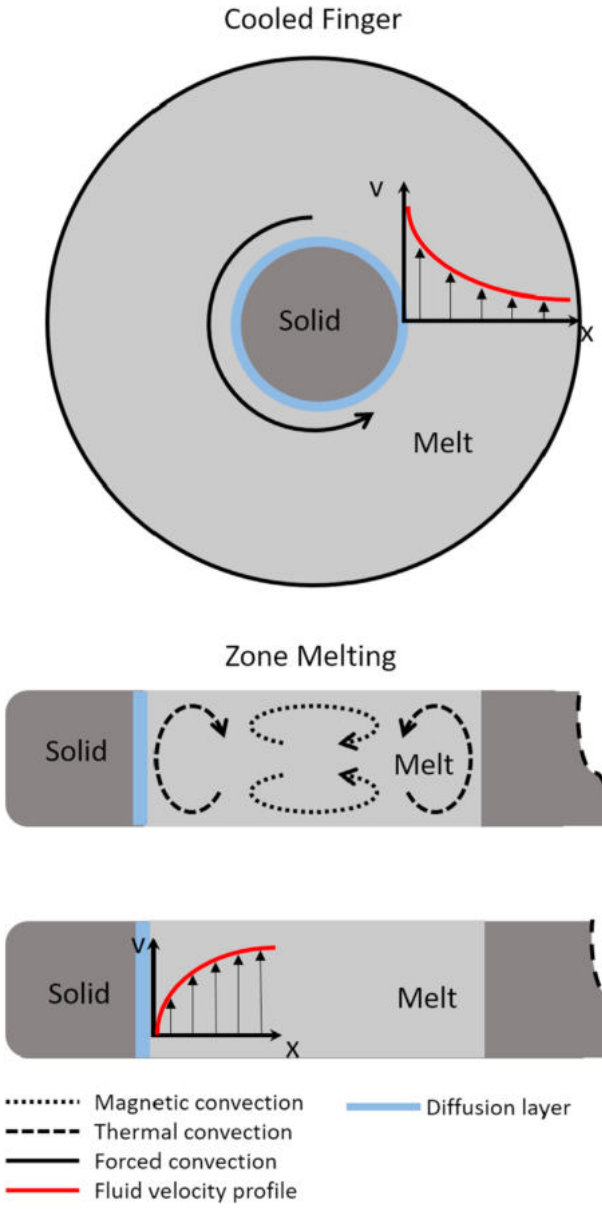

Fig. 3 – Types of convection and fluid velocity profile in cooled finger and zone melting.

2. Objectives and experimental methodology

The aim of this paper is to experimentally demonstrate the purification effect caused by different types of convection from these two fractional crystallization techniques. In order to achieve that, the growth rate (as an influencing parameter for segregation of impurities) will be kept at a fixed range.

Moreover, the common characteristics among the fractional crystallization equipment; i.e. growth rate, thermal gradient and purification rate, were investigated in this work to identify the main mechanisms behind the purification within each technique.

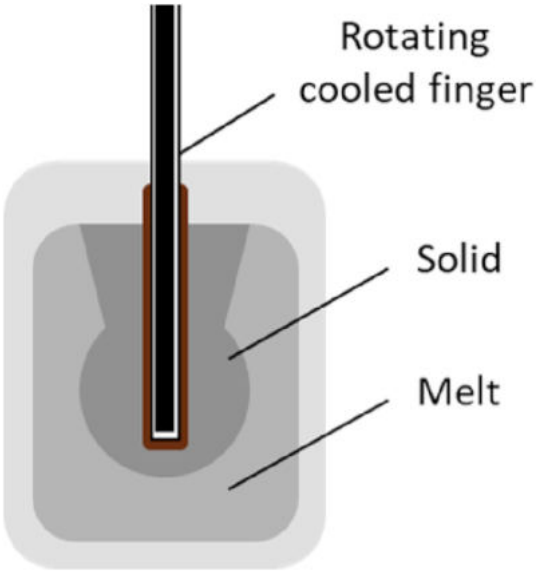

Fig. 4 – Cooled finger schematic.

In total, 25 cooled finger and 10 zone melting experiments with different parametric configurations were performed. Their samples were chemically analyzed via spark spectroscopy (Optical Emission Spectroscope, Spectro Analytical Instruments, Kleve, Germany), which has a certified measurement precision up to 4N5 (99.995 wt.%) for aluminum. To enable the analytical results within the precision limits of the used spark spectrometer, an artificial initial material was created by alloying 4N8-purity aluminum with 0.1 wt.% of Fe, Si and Pb.

2.1. *Experimental setup and process parameters*

Zone melting and cooled finger were the fractional crystallization techniques investigated in this paper, both available at the IME Institute of RWTH Aachen University. A description of the employed equipment is summarized in this section.

2.1.1. *Cooled finger*

The cooled finger purification equipment is installed in an open resistance furnace with a PID temperature controller. It is also coupled to a frequency controlled electric motor that drives the cooled finger rotation. A schematic of the cooled finger setup can be seen on Fig. 4. The rotational speed of the motor and the cooling fluid flow rate were selected as variables. The flexibility of its operation relies on the wide range of adjustment and variable combination [15,25].

The cooled finger trials were performed with an initial melt temperature of 700 °C. Subsequently to the immersion of the cooled finger into the molten bath, the cooling gas flow and rotation were initiated. These two parameters are the main factors influencing purification. The rotation was varied from 25 to 100 RPM, and the cooling gas flow rates from 45 to 70 L min^{-1} at 2 bar of pressure using compressed air.

The process starts by inserting the cooled finger in a molten bath, where after a period of time a layer of purified metal starts to slowly grow over the cooled finger surface.

During the solidification, the segregation of impurities occur and the solidified fraction of metal will have a lower impurity content than the bulk metal remaining in the crucible. Samples were taken from the melt prior to the cooled finger immersion (C_0), the crystallized material over the cooled finger (C_S), and the residual melt in the crucible (C_L).

The melt temperature was recorded during the experiments to determine the solidification time and calculate the growth rate with it. Additionally, one set of experiments was performed to measure the temperature gradient necessary for solidification.

2.1.2. *Zone melting*

The zone melting equipment consists of an induction heating coil which travels along a surrounded vacuum tight quartz tube, where the aluminum containing crucible is held by water cooled supports inside the chamber. A schematic of the zone melting setup can be seen on Fig. 5. The zone melting equipment, employed for these experiments, is retrofitted with an infrared camera, which enables the measurement of the molten zone length and temperature during the refinement process. The coil movement velocity (0.8 and 1.2 mm min^{-1}) and the number of passes (1 and 3 passes) were selected as variables. The supplied power to the induction coil was fixed to 10 kW for all the trials. The growth rate and thermal gradient data, was obtained through the infrared camera as detailed in [26,27].

In preparation for the experiments, aluminum was cast to fit the graphite long crucibles also known as "boats". These were sprayed with a thin layer of high purity boron nitride to prevent the aluminum adhesion during the process. The boats were then positioned with an inclination angle of 1° inside the chamber, to prevent the mass transport towards the process-end side of the bar. To prepare the argon inert atmosphere, the chamber was evacuated and flushed twice with argon before setting it at 700 mbar.

The refined bars were cut and polished at specific lengths to proceed with the chemical analysis through spark spectroscopy. Later, the real growth rate was calculated based on the tracking of the growth front obtained by analyzing the temperature profile via the infrared camera. This method allow a better understanding of the process, rather than assuming the movement velocity of the induction coil as a nominal unchangeable value.

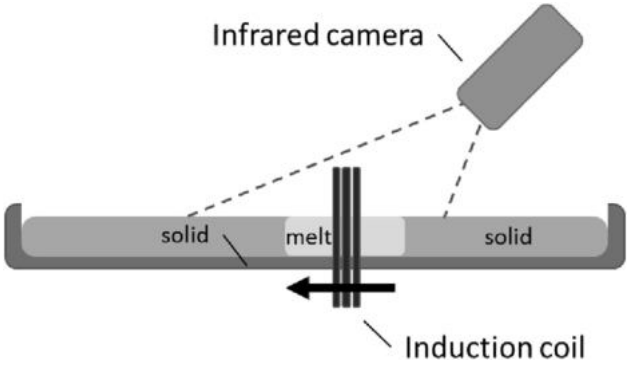

Fig. 5 – Zone melting schematic.

2.2. *Methodologies*

2.2.1. *Measurement of the temperature gradient*

2.2.1.1. *cooled finger*. The temperature gradient measured in the Cooled Finger trials was based on the difference between the temperature at the solidification front with respect to the melt during the purification process. These temperature values were recorded by localizing four thermocouples at specific distances across the crucible. In these experiments, the crystal was allowed to grow over the first set of thermocouples (as seen on Fig. 6) while recording their values. The time required for the crystal to grow over the first set of thermocouples was defined from previous trials. The temperature gradient measurements were performed without rotation.

2.2.1.2. *Zone melting*. For the temperature gradient measurements in the zone melting process, a thermographic analysis was computed from the infrared camera recordings (Fig. 7).

In order to record the zone melting process through the quartz tube, the infrared camera (IR) measures radiation in the spectral range between 0.78 and 1.1 μm. The IR camera is fixed in a way that it moves along with the induction coil. The camera's software was calibrated for lightly oxidized aluminum sample, as described in Reference [26].

By plotting the measured temperature along the crucible length, it is possible to obtain the temperature gradient ($\Delta T/\delta x$) for each measured frame, as seen in the example from Fig. 8.

2.2.2. *Calculation of the average growth rate*

2.2.2.1. *Cooled finger*. To determine the average growth rate, the sample wall thickness was divided by the crystallization time. To measure the crystallization time, the melt temperature was recorded employing a thermocouple placed inside

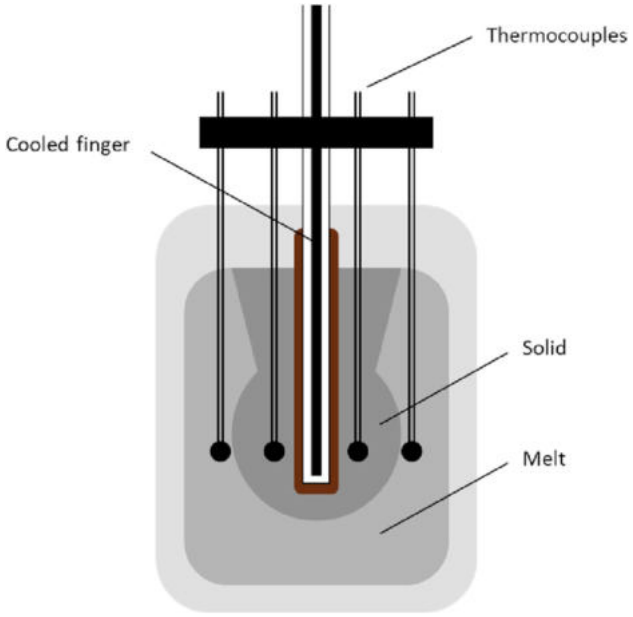

Fig. 6 – Cooled finger temperature gradient measurement setup.

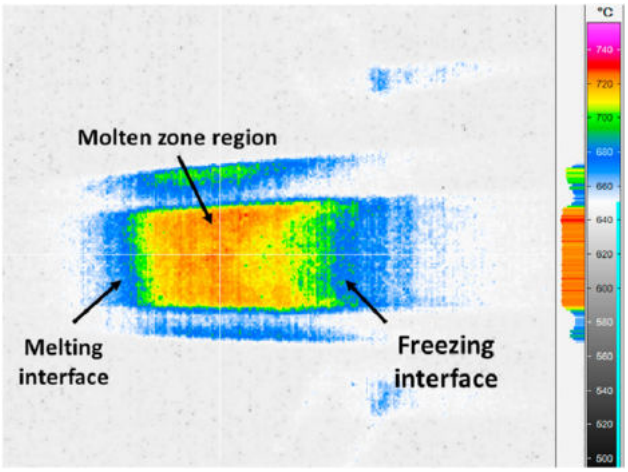

Fig. 7 – Thermograph of an Al-sample during zone melting process.

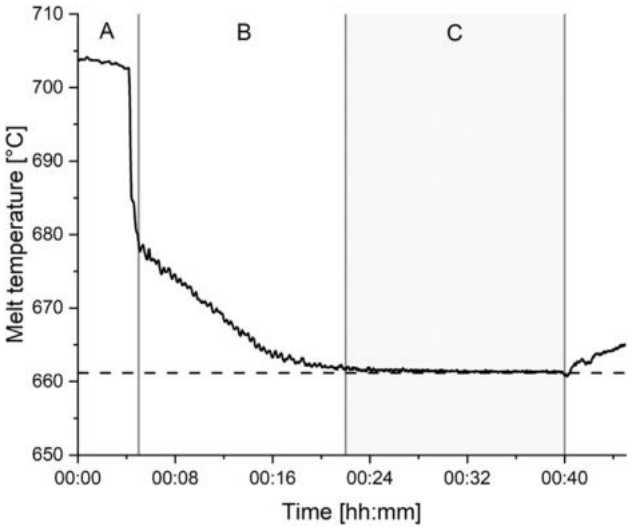

Fig. 9 – Example of a solidification time measurement from a cooled finger experiment.

the melt, adjacent to the crucible wall at the same height of the graphite body. An example of a typical temperature recording can be seen in Fig. 9.

Within this profile, one can point out three stages: Firstly, the moment, in which the cooled finger is immersed into the molten bath (region A), immediately after, the slow drop in melt temperature induced by the heat extraction from the cooled finger (region B), and during the solidification process, the constant temperature plateau located slightly above the melting point of aluminum, indicating the crystallization phase (region C).

2.2.2.2. *Zone melting*. The average growth rate for this case, is obtained by considering the coil movement velocity and the actual freezing interface movement. In the experiments performed for this comparison, two different movement velocities were investigated, 0.8 mm/min (13 microns/sec) and 1.2 mm/min (20 microns/sec).

Although the averaged growth rate lies close to the selected velocities, the growth rate varies along the process due to the molten zone length change. For this purpose, the camera recording was analyzed in a frame-by-frame manner to compute the actual growth rate throughout the refinement process. A typical graph of the growth rate change along the crucible can be seen on Fig. 10.

The increased size of the molten zone length at the beginning and end of the process causes higher growth rates at those instances. This is due to the geometric shape of the graphite boat, that acts as an additional susceptor mass, resulting in an increased heat input to the molten aluminum. For the same reason, the section between the two valleys seen in the middle portion of the bar corresponds to a necessary power adjustment to maintain the zone length steady during the process.

2.2.3. *Calculation of the purification ratio*

The chemical composition of all aluminum samples was analyzed via spark spectrometry. Each sample was measured

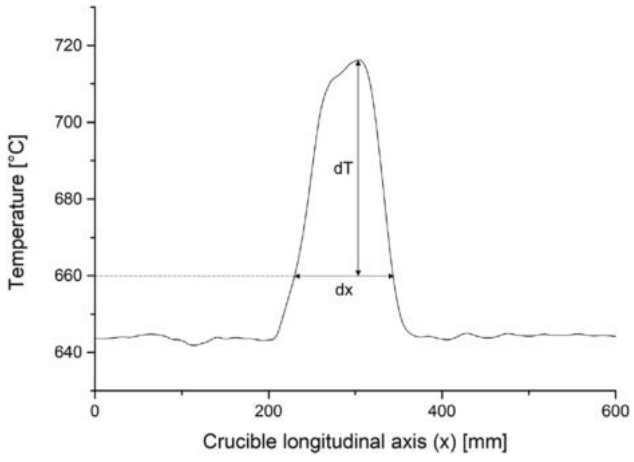

Fig. 8 – Zone melting temperature gradient measurement.

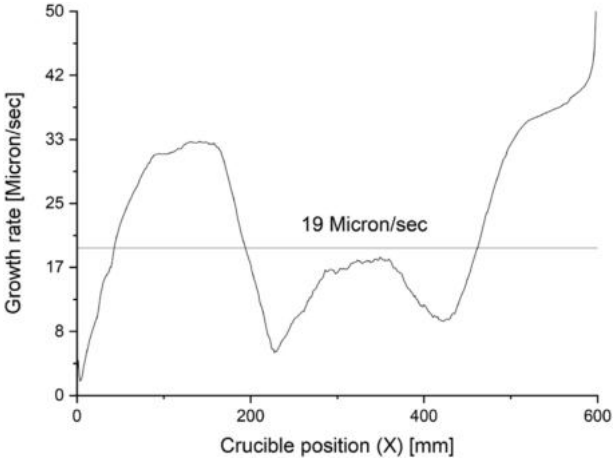

Fig. 10 – Growth rate variation along the zone melting process.

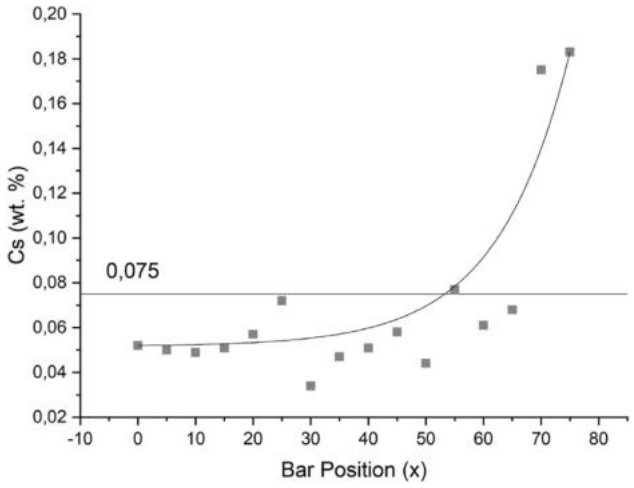

Fig. 11 – Typical solute distribution after zone melting for an initial 0.075 wt. % solute concentration.

three times to assure reproducibility. The average of these measurements was considered to calculate the purification ratio.

2.2.3.1. *Cooled finger*. Throughout the Cooled Finger trials, a sample of the initial melt (C_0) and from the residual melt in the crucible (C_L) were collected. Additionally, the crystallized material (C_S) was also sampled. To achieved purification was then calculated based on the percentage of the solute removal for each individual impurity, and defined according to Eq. (4) below.

$$\text{Purification}(\%) = \left(1 - \frac{C_S}{C_0}\right) \cdot 100 \quad (4)$$

2.2.3.2. *Zone melting*. For the zone melting trials, the initial solute concentration of the bars was obtained before the trials (C_0). After concluded the defined number of zone refining passes, the bars were cut at equally spaced distances to perform the chemical analysis of C_S as well as to perform the concentration profile along the bar, as predicted from the Scheil distribution theory (see Fig. 11 This data was employed to determine the most favorable compromise between refinement and yield, to define the average purification ratio. The value of C_S is then considered as the average concentration within the first two thirds of the bar, deemed as the product.

2.2.4. *Influence of process parameters*

2.2.4.1. *Cooled finger*. To evaluate the effect of the cooling gas flow-rate and rotation rate, as the main process parameters for the cooled finger, a series of trials were conducted as following.

To investigate the effect of cooling gas flow rate on the growth rate and purification, the rotation rate was fixed to 25 RPM as shown in Table 2.

To investigate the effect of rotation on the growth rate and purification, the cooling rate was fixed to 70 L/min as shown in Table 3 below.

Table 2 – Investigated cooling gas flow-rate parameters at 25 RPM.

Cooling gas flow rate (Liter/min)				
45.0	47.5	50.0	52.5	55.0

Table 3 – Investigated rotation rate parameters at 70 L/min.

Rotation rate (RPM)				
60	70	80	90	100

2.2.4.2. *Zone melting*. To analyze the impact of the coil movement velocity and the number of passes, as the most important process parameters in the zone melting, a series of experiments employing two different velocities; 1.2 and 0.8 mm/min, were performed in combination with a one-as well as 3-Pass refining sequences, respectively.

3. Results and discussion

The impurity segregation in any fractional crystallization technique is mostly influenced by the growth rate and the thickness of the diffusion layer ahead of the solidification interface.

The effect of the temperature gradient is different on each of the investigated techniques. In this section, it is demonstrated that convection plays an important role in purification.

3.1. *Growth rate*

3.1.1. *Cooled finger*

In the case of the cooled finger, higher growth rates are achieved by increasing the cooling rate. More precisely, this air flow creates the required temperature gradient to keep the crystallization process. Fig. 12 depicts the relationship between the cooling rate and the growth rate at a constant rotational speed plotted with a linear fit.

Additionally, the rotational speed of the cooled finger plays an important role on the growth rate regulation. Fig. 13 shows how the higher rotational speeds - at a constant cooling rate- promotes lower growth rates.

The results from Figs. 12 and 13 shows that the chosen process parameters were able to generate a growth rate within the target range (10–20 microns/sec).

3.1.2. *Zone melting*

Generally, the zone melting uses the coil movement velocity to control the growth rate. However, the actual growth rate is the sum of the coil movement velocity and the zone length variation. Fig. 14 shows how the growth rate varies around a fixed coil movement velocity of 1.2 mm/min (20 microns/sec). The growth rate fluctuation is mainly attributed to the zone length variation along the process.

Although strongly dependent on the zone length, the average growth rate lies close to the coil movement velocity. Fig. 15 shows the growth rate variation over the crucible length at two different selected coil movement velocity: 1.2 (20

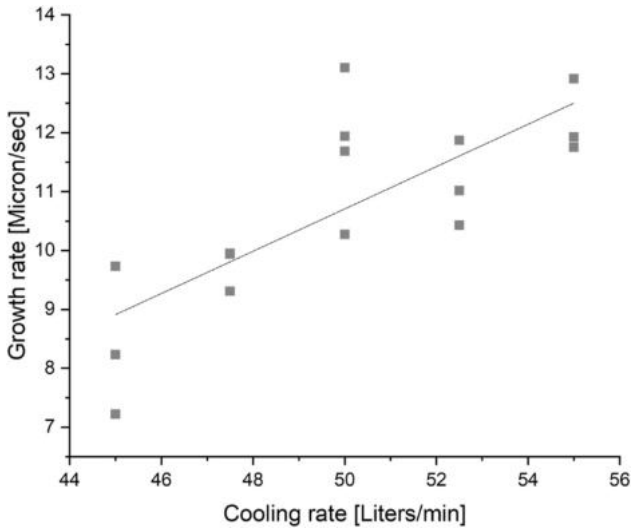

Fig. 12 – Effect of cooling gas flow-rate on the growth rate at 25 RPM.

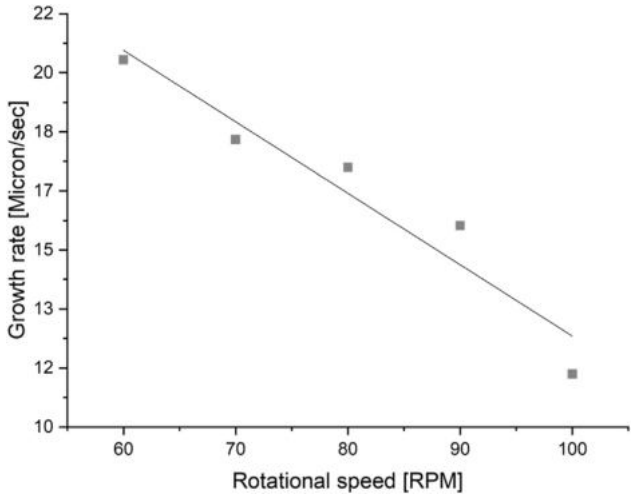

Fig. 13 – Effect of rotational speed on the growth rate at a cooling rate of 70 L min^{-1}.

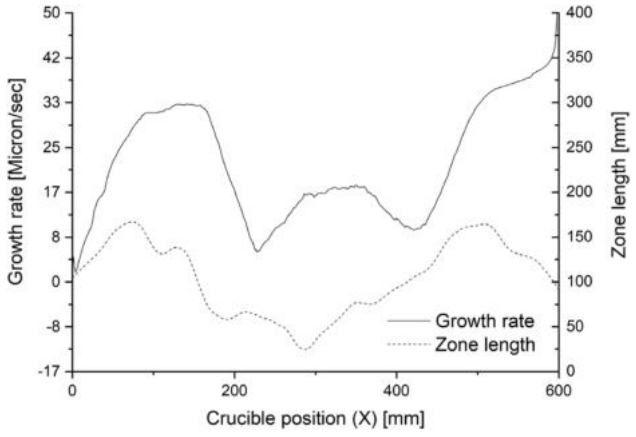

Fig. 14 – Growth rate and zone length variation along the zone melting process for a fixed coil movement velocity of 1.2 mm/min.

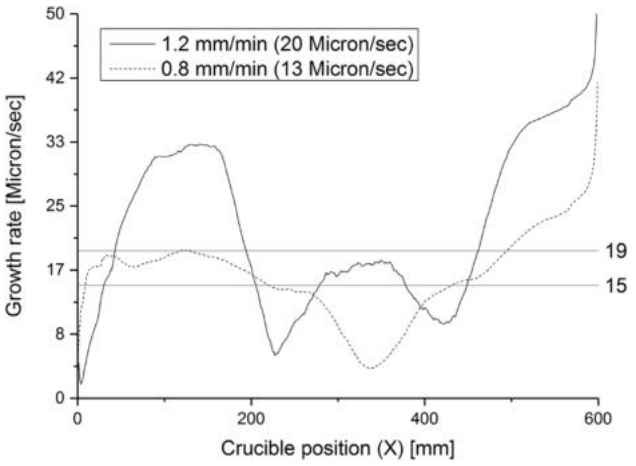

Fig. 15 – Growth rate variation of the two investigated coil movement velocities.

microns/sec) and 0.8 mm/min (13 microns/sec). After calculating the average growth rate during the zone melting process (shown with the horizontal lines), the resulting values do not deviate more than 2 microns/sec from the constant coil movement velocity.

The relationship between the average growth rate in both processes posses a markedly effect on the purification. In the cooled finger trials, the growth rate is mainly controlled by the air cooling and rotational speed. On zone melting however, the growth rate is set by a combination of two factors, the coil movement velocity as well as the zone length variation.

3.2. *Purification*

Besides growth rate, purification is strongly dependent on the diffusion layer thickness. The role of forced convection on the reduction the diffusion layer thickness results in an increase of the purification.

3.2.1. *Cooled finger*

The cooled finger purification results show an improved impurity rejection as the average growth rate increases. The previous in accordance with the BPS theory. Fig. 16 shows the decrease in purification ratio as the average growth rate increases, focusing on lead as an impurity in aluminum, at cooling rates varying from 45 to 55 L min^{-1}, while maintaining a fixed rotation of 25 RPM. As depicted by the linear trend line, purification ratio from 55 and up to 75% are expected from the cooled finger around a growth rate of 10 microns per second.

The role of rotation within the cooled finger is to decrease the diffusion layer thickness through forced convection. What distinguishes the cooled finger from zone melting is that the highest fluid flow velocity takes place at the solidification interface. Fig. 17 shows the direct relationship of the rotation on the purification ratio of Fe and Si as impurities in aluminum.

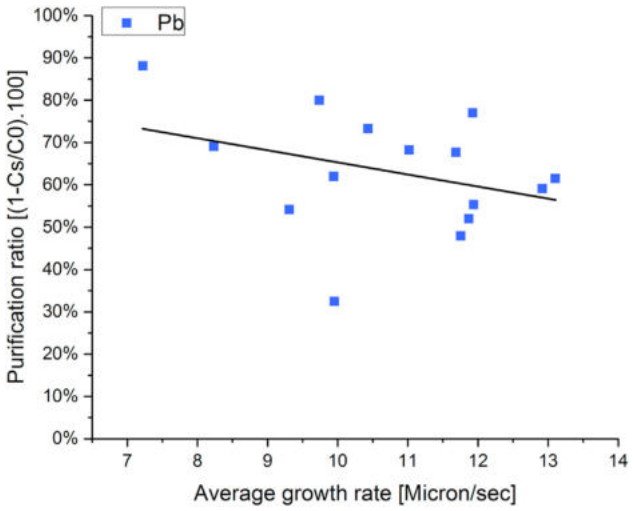

Fig. 16 – Effect of the growth rate on the purification ratio.

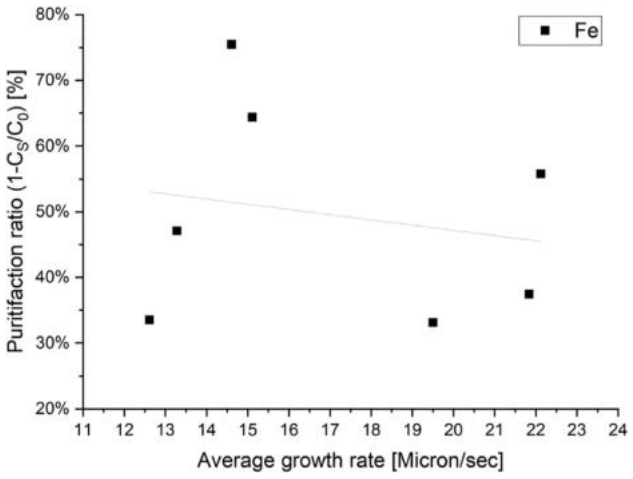

Fig. 18 – Effect of the coil speed (growth rate) on the purification ratio of Fe in aluminum.

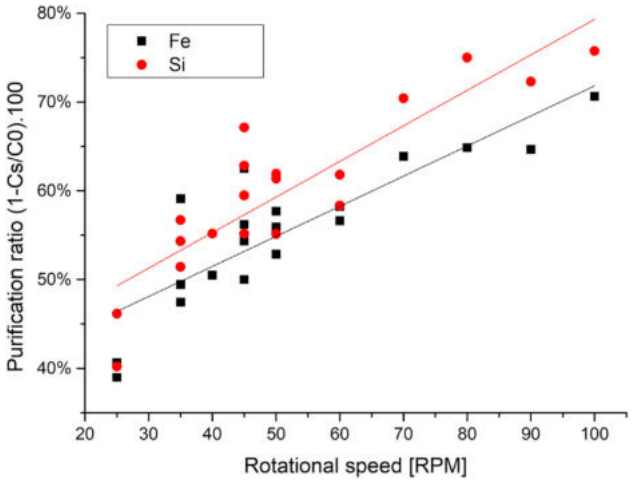

Fig. 17 – Effect of rotation rate on purification ratio of Fe and Si in aluminum at cooling rates varying from 50 to 70 L min^{-1}.

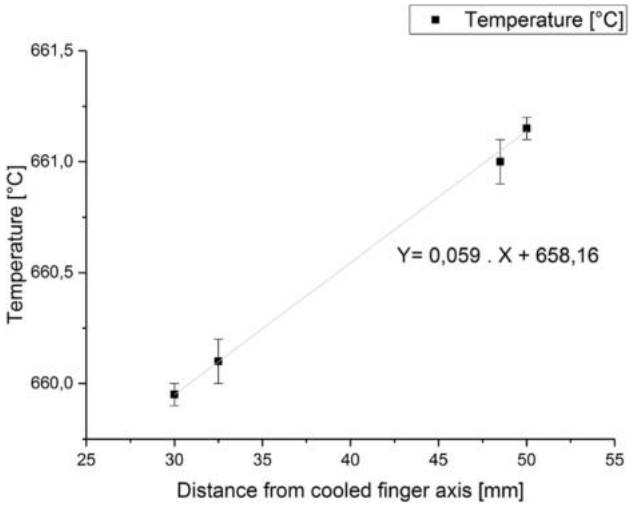

Fig. 19 – Cooled finger temperature gradient.

3.2.2. *Zone melting*

The zone melting trials show improved purification rates at lower growth rates. To be able to calculate the purification ratio, two thirds of the zone refined bar were considered as the purified product.

The two levels of coil movement velocity employed during the zone melting trials are shown in Fig. 18. From the 1-Pass refined samples, the purification ratio increases as the average growth rate is reduced, focusing on iron as an impurity in aluminum. The linear trend line shows that average purification ratios from 40 and up to 55% are expected from the 1-Pass zone melting process employing a coil speed of 0.8 mm/min (13 microns/sec) and 1.2 mm/min (20 microns/sec) respectively.

The decrease in the diffusion layer thickness is achieved by the thermal and electromagnetic convection caused by the highly localized heat input induced by the induction coil. This results in a high temperature gradient along the molten zone.

3.3. *Temperature gradient*

3.3.1. *Cooled finger*

The experimental measurements of the temperature gradient for the cooled finger trials showed that the melt temperature increases slight from the vicinity of the cooled finger, towards the crucible wall. The temperature difference measured at the solid–liquid interface was 0.06 °C/mm, which established the strong dependence of the process even on the slightest changes in its setup parameters such as furnace temperature, insulation, cooling gas flow rate and rotation.

It is worth mentioning (as described in section 2.2.1) that the measurements of temperature gradient were performed in a static condition i.e. without rotation. Its effect would further decrease the temperature gradient value due to the mixing of the melt. Fig. 19 shows the temperature profile measured around the cooled finger during the crystallization process.

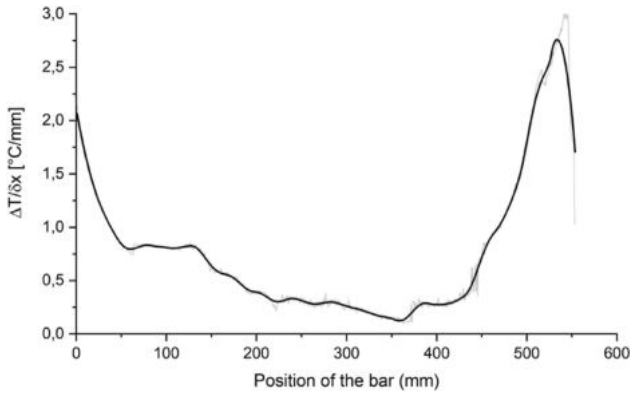

Fig. 20 – Zone melting temperature gradient variation.

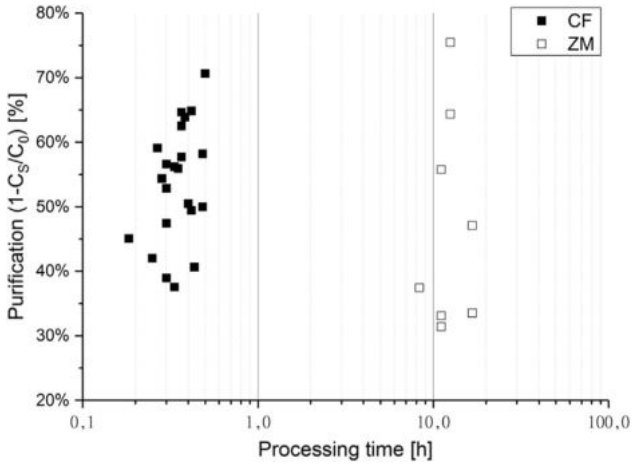

Fig. 21 – Cooled finger and zone melting purification results against processing time.

3.3.2. *Zone melting*

The temperature gradient in zone melting was computed from the thermographs captured throughout the experiments and plotted as a temperature profile in Fig. 20. The temperature gradient throughout the zone melting process is strongly dependent on the graphite crucible, which acts as a susceptor transferring the heat generated by the electromagnetic field of the coil to the aluminum.

In contrast to the cooled finger, where a slight temperature gradient drives crystallization, the zone melting process experiences a wide range of temperature gradients along its processing. These variations were measured to lie between 0.2 and 3.0 °C/mm along all the experiments performed, which can reach up to 50 times the value observed in the cooled finger trials.

3.4. *Competitive advantage of the cooled finger*

If any parameter stands out as a strong differentiating characteristic between the cooled finger and the zone melting techniques, is their processing time. The cooled finger requires less than an hour to achieve an impurity removal ratio of up to 80 wt.% with a 40–60% yield, while zone melting needs from 8 to 17 h to achieve similar results, depending on the number of passes and coil speed. Fig. 21, shows the range of purification in dependence of the processing time required by cooled finger and zone melting.

4. Conclusions

The cooled finger and zone melting are both based on the principle of fractional crystallization. The growth rate (as demonstrated by Scheil and BPS) stands as a critical parameter for the obtained solute segregation during crystallization. Lower growth rates will allow a better segregation of solutes from the crystallization interface towards the bulk melt.

It was successfully demonstrated that the cooled finger has a higher competitive advantage over zone melting. While both techniques are capable of purifying aluminum at similar growth rates, the cooled finger design favors the segregation of impurities. Overall, the cooled finger has the following advantages over zone melting:

1) The possibility to promote a forced convection ahead of the solidification interface, which -according to solute segregation theory-improves solute segregation without affecting the growth rate, resulting in a reduced processing time.
2) The solid growth rate in cooled finger has a better stability than zone melting. The first technique is influenced mainly by the cooling gas flow and rotation, while the second is subjected to the fluctuations in the zone length along the process.

The difference between the temperature gradient in the cooled finger and zone melting can be explained by its role in each process. The solidification in cooled finger is driven by the temperature gradient while in zone melting it is driven by the coil movement and the zone length variation.

The temperature gradient measured in the cooled finger of 0.06 °C/mm indicate a minimal effect of thermal convection, while for zone melting the higher temperature gradients between 0.2 and 3.0 °C/mm are clear indication that thermal convection is the main driver for mixing in the molten zone.

The trials conducted with the cooled finger showed an impurity removal ratio of around 80% for Pb, 70% for Fe and up to 75% for Si. For the zone melting trials, up to 75% of Fe was removed after 3 passes of zone melting.

Despite the preference of the zone melting process over the cooled finger due to its automation simplicity, the lower processing times offered by the cooled finger makes it the perfect candidate for up-scaling projects within the metal refining industry.

Author contributions

Bernd Friedrich was the principal investigator. Danilo C. Curtolo and Semiramis Friedrich conceived and designed the experiments. Danilo C. Curtolo and Martin J. Rodriguez R. performed the experiments. Semiramis Friedrich, Danilo C. Curtolo and Martin J. Rodriguez R. analyzed the data. Danilo C.

Curtolo, Martin J. Rodriguez R. and Semiramis Friedrich wrote and edited the manuscript.

Declaration of Competing Interest

The authors declare no conflict of interest.

Acknowledgments

The authors thanks the CNPQ-Brazilian National Council for Scientific and Technological Development for the financial support of Danilo C. Curtolo.

REFERENCES

[1] Hoshikawa H, Tanaka I, Megumi T. Refining technology and low temperature properties for high purity aluminum. Sumitomo Kagaku 2013:1–12.
[2] Mikubo S. The latest refining technologies of segregation process to produce high purity aluminum. In: 12th international conference on proceedings of the 12th international conference on AluminiumAlloys; 2010. p. 224–8.
[3] Dawless RK, Troup RL, Meier DL, Rohatgi A. Production of extreme-purity aluminum and silicon by fractional crystallization processing. J Cryst Growth 1988;89(1):68–74. https://doi.org/10.1016/0022-0248(88)90073-5.
[4] Kondo M, Maeda H, Mizuguchi M. The production of high-purity aluminum in Japan. JOM (J Occup Med) 1990;42(11):36–7. https://doi.org/10.1007/BF03220434.
[5] Jabbour GE, Kippelen B, Armstrong NR, Peyghambarian N. Aluminum based cathode structure for enhanced electron injection in electroluminescent organic devices. Appl Phys Lett 1998;73(9):1185–7. https://doi.org/10.1063/1.122367.
[6] Bochkarev MN, Katkova MA, Ilichev VA, Konev AN. New cathode materials for organic light-emitting diodes: Tm:Yb and Eu:Yb. Nanotechnologies in Russia 2008;3(7–8):470–3. https://doi.org/10.1134/S1995078008070094.
[7] Ohtaki M, Kudou H. Application of some vacuum distillation process to refine Zn from Al scrap. 1998.
[8] Johnson AF. Aluminum production. 1966. URL, http://aluminium.org.au/flowchart/flowchart.html.
[9] Hollingshead E, Phillips N. Subhalide distillation of aluminum. 1943.
[10] Scheuer E. Distillation of aluminum from aluminum alloys. 1953.
[11] Wei QS, Yang B, Li YF, Dai YN. Zinc removing from aluminum alloy by vacuum distillation. Adv Mater Res 2011;402:303–6. https://doi.org/10.4028/www.scientific.net/amr.402.303.
[12] Loutzenhiser PG, Guglielmini E, Frei A, Steinfeld A. Vacuum distillation of aluminum and silicon via carbothermal reduction of their oxides with concentrated solar energy. 2011.
[13] Zhao H, Lu H. The development of 85kA three-layer electrolysis cell for refining of aluminum. ©2009. In: Light metals; proceedings of the technical sessions presented by the TMS Aluminum Committee at the TMS 2008 annual meeting & exhibition, Warrendale, Pa. : minerals, Metals and Materials Society. USA: New Orleans; 2008. p. 533–40. Louisiana.
[14] Hurle D. Constitutional during growth from stirred melts - I theoretical. Solid State Electron 1961;3:37–44.
[15] Curtolo D, Friedrich S, Bellin D, Nayak G, Friedrich B. Definition of a first process window for purification of aluminum via "cooled finger" crystallization technique. Metals 2017;7(9):341. https://doi.org/10.3390/met7090341. URL, http://www.mdpi.com/2075-4701/7/9/341.
[16] Burton Ja, Prim RC, Slichter WP. The distribution of solute in crystals grown from the melt. Part II. Experimental. J Chem Phys 1953;21(11):1991–6. https://doi.org/10.1063/1.1698729. URL, http://link.aip.org/link/JCPSA6/v21/i11/p1987/s1&Agg=doi.
[17] Burton JA, Prim RC, Slichter WP. The distribution of solute in crystals grown from the melt. Part I. Theoretical. J Chem Phys 1953;21(11):1987. https://doi.org/10.1063/1.1698728.
[18] Ostrogorsky A. Empirical correlations for natural convection, Δ and keff. J Cryst Growth 2015;426:38–48. https://doi.org/10.1016/j.jcrysgro.2015.04.017.
[19] Chatelain M, Albaric M, Pelletier D, Botton V. Solute segregation in directional solidification: scaling analysis of the solute boundary layer coupled with transient hydrodynamic simulations. J Cryst Growth 2015;430:138–47. https://doi.org/10.1016/j.jcrysgro.2015.08.013. URL https://doi.org/10.1016/j.jcrysgro.2015.08.013.
[20] Povinelli ML, Korpela SA, Chait A. Solute boundary layer on a rotating crystal. J Cryst Growth 1994;144(1–2):103–6. https://doi.org/10.1016/0022-0248(94)90017-5.
[21] Abramov O, Teumin I, Filonenko V, Eskin G. The effect of ultrasound on the process of naphthalene zone melting. Akusticheskij Zhurnal 1967;13(2):161–9.
[22] Watanabe M, Eguchi M, Wang W, Hibiya T, Kuragaki S. Controlling oxygen concentration and distribution in 200 mm diameter Si crystals using the electromagnetic Czochralski (EMCZ) method. J Cryst Growth 2002;237–239(1 4 III):1657–62. https://doi.org/10.1016/S0022-0248(01)01824-3.
[23] Shingu H, Arai K, Sakaguchi M, Nishide T, Watanabe O, Otsuka R, et al. Process for producing high-purity aluminum. 1984.
[24] Shevchenko N, Roshchupkina O, Sokolova O, Eckert S. The effect of natural and forced melt convection on dendritic solidification in Ga-In alloys. J Cryst Growth 2015;417:1–8. https://doi.org/10.1016/j.jcrysgro.2014.11.043. URL https://doi.org/10.1016/j.jcrysgro.2014.11.043.
[25] Friedrich S, Curtolo D, Friedrich PB. Investigation of temperature effect on impurities distribution coefficient in molten aluminum through theoretical calculation and experimental fractional crystallization. In: EMC - European metallurgical conference. Leipzig - Germany: GDMB; 2017. p. 889–96.
[26] Curtolo D, Zhang X, Rojas M, Friedrich S, Friedrich B. Realization of the zone length measurement during zone refining process via implementation of an infrared camera. Appl Sci 2018;8(6):875. https://doi.org/10.3390/app8060875. URL, http://www.mdpi.com/2076-3417/8/6/875.
[27] Zhang X, Friedrich S, Friedrich B. Characterization and interpretation of the aluminum zone refining through infrared thermographic analysis. Materials 2018;11(10):2039. https://doi.org/10.3390/ma11102039. URL, http://www.mdpi.com/1996-1944/11/10/2039.